INAF-Osservatorio astrofisico di Torino
Technical Report nr. 174

Implementation of a CME flag for METIS: further tests on various transient emission sources

Alessandro Bemporad

Pino Torinese, 15 dicembre 2016

IMPLEMENTATION OF A CME FLAG FOR METIS:
FURTHER TESTS ON VARIOUS TRANSIENT EMISSION SOURCES

A. Bemporad – INAF-Turin Astrophysical Observatory

ABSTRACT

The aim of the work described here is to characterize the evolution of visible light (VL) emission detected in coronagraphic images and associated with transient features alternatives to Coronal Mass Ejections (CMEs). The target is to verify how far the automatic CME detection algorithm under development for Metis onboard Solar Orbiter will be able to reject these events and raise the flag only in the occurrence of real CMEs. Results based on the analysis of STEREO/COR1 sequences of polarized images show that the presence of spikes due to cosmic rays (or Solar Energetic Particles – SEPs) and the transit of planets will give a negligible contribution to the intensity averaged over angular sectors. On the other hand the transit of a bright comet (like the Lovejoy) will provide a significant transient emission raising the CME flag. Possible strategies to solve this problem are proposed. Moreover, comparative analysis of STEREO/COR1 and SOHO/LASCO-C2 data shows that relative intensity variations on C2 are much larger than those observed on COR1 for the same objects (CMEs or planets), because of significant differences between the two instruments. Hence, definition of reliable values for the threshold value in the algorithm activating the "CME flag" likely will be possible only after the launch of Solar Orbiter, when first Metis data will be available.

Summary

Index of figures

Index of tables

1. Introduction

The aim of the work being described here is to characterize the temporal variations of intensities detected in sequence of coronagraphic images acquired during the occurrence of different peculiar "events". This study has been conceived in the framework of the development of an automatic algorithm for the detection of Coronal Mass Ejections (CMEs) to be implemented for the Metis coronagraph onboard Solar Orbiter. Typical properties of the intensity evolutions observed during a typical "standard" and "halo" CME have been already described in a previous report. The problem I want here to deal with is to understand how far a CME detection algorithm based on simple running differences could be able to make also a distinction between a "real CME" and other possible phenomena like

- the occurrence of a Solar Energetic Particle (SEP) storm,
- the transit of a planet in the instrument Field of View (FOV),
- the transit of a comet in the instrument FOV.

To this end, sequences of coronagraphic images acquired by the COR1 telescopes onboard STEREO–A and –B spacecraft have been downloaded and analyzed. Each sequence of polarized COR1 observations typically consists of triplets of images acquired with 3 different orientations of the linear polarizer (0°, 120° and 240° measured counterclockwise from the solar North). Every single image is acquired with a time interval of 12 seconds (single exposure time of ~ 1.7 seconds), while every triplet is acquired with time interval of 5 minutes. Images have dimensions of 512x512 pixels, with nominal spatial resolution by 3,7 arcsec/pixel, or 1024x1024 pixels, depending on the period of the STEREO mission. Hence, everyday a total of 864 polarized images are acquired, corresponding to 864/3 = 288 polarization triplets per day.

In the next paragraph (§2) I describe the selected events, the observation intervals, and the analysis performed on the data. The following paragraphs then describes results obtained for the observation of a SEP event (§3), the transit of a planet (§4) and of a comet (§5) in the instrument FOV. After a comparison between STEREO/COR1 and SOHO/LASCO data relative to the same astronomical objects (§6), conclusions are given in the last paragraph (§7).

2. Selected events and description of the analysis

The observational periods have been selected starting from the most spectacular events reported in the section "galleries" of the official STEREO homepage (http://stereo.gsfc.nasa.gov/gallery/gallery.shtml). The selected events and observation periods are listed in *Table 1*, together with the number of frames analyzed.

In particular, for the SEP event I selected the big solar eruption that occurred on March 21, 2011 starting from 02:06 UT. At that time the STEREO spacecraft were almost in quadrature with the Earth, hence flares occurring on the East (West) quadrant as observed by STEREO-B (STEREO-A) are not observed on Earth, because they occur in the unobserved hemisphere. For this reason, the strong flare associated with this eruption is not classified in flare catalogues. In any case, COR1 images acquired by STEREO-A are clearly affected by a strong SEP flux starting from about 03:06 UT, hence about 1 hour after the flare. This is related with the location on the disk of the source Active Region, which is at a longitude of about 40°W (as seen by STEREO-A), likely connected via the Parker-spiral with the spacecraft. After the flare, a huge limb CME is also observed by STEREO-A expanding on the North-West quadrant.

Event description	Satellite	Start time	End time	Polarized exp.
CME (standard) followed by SEP bombardment	STEREO-A	2011/03/21, 00:05:00	2011/03/21, 14:55:18	537 (280 MB), 512X512 pix^2
Planet (Jupiter) transit	STEREO-B	2009/03/15, 09:05:00	2009/03/16, 16:55:18	576 (1,13 GB), 1024X1024 pix^2
Comet (Lovejoy) transit	STEREO-B	2011/12/15, 16:00:00	2011/12/16, 15:55:18	861 (449 MB), 512X512 pix^2

Table 1: List of the specific events and observation periods for the data analyzed here.

For the planet transit I selected the Jupiter transit through the COR1 instrument FOV that was observed by STEREO-B on March 15 – 18, 2009. The planet is very well observed (together with the 4 Galileian moons, very well visible in the 1024x1024 images): it enters in the FOV on March 15 around 10:45 UT at the East limb, then it moves from East to West temporarily disappearing behind the occulter between March 16, 14:35 – 23:55 UT, and finally leaving the instrument's FOV on March 18, 04:45 UT. No significant solar eruptions occurred during the transit of the planet.

For the comet transit I selected the Lovejoy comet, that was very well observed by the STEREO-B COR1 coronagraph on December 15 – 16, 2011. The comet nucleus enters in the STEREO-B/COR1 FOV on December 15, around 21:05 UT in the South-West quadrant and then, moving almost radially towards the Sun, the nucleus disappears behind the instrument occulter on 23:05. Then the nucleus reappears again, still on the South-West quadrant but moving away from the Sun, on December 16, 05:25 UT, finally leaving the STEREO-B/COR1 FOV around 10:45 UT. The comet then survives his close encounter around the Sun releasing a very bright tail which is observed by STEREO-B/COR1 also on the North-East quadrant as the comet transits around his perihelion. No significant solar eruptions occurred during the transit of the comet.

For each sequence, images have been loaded and calibrated in IDL by using the standard routines provided in Solar-Software within the "SECCHI" package (with SCCREADFITS and COR1_CALIBRATE). Moreover, each triplet of polarized images has been used to derive the total brightness (tB) and polarized brightness (pB) images (with COR1_QUICKPOL). An IDL routine to perform these calibrations and analyses to each one of the images has been written: the routine then extract from every image the intensity averaged over 6 angular sectors, each one with angular extension of 60°, radial extension between 1.7 and 3.7 R_{sun}. In the 512x512 images the total number of pixels per angular sector is around $N_{pix} \sim 2.316\times10^4$ pix, corresponding to about 8.8% of the total image. Hence, these 6 angular sectors cover overall the ~ 53% of the whole image.

The intensities measured in each sector are summed pixel by pixel; hence, in what follows, the absolute intensities will be given in units of $1/B_{sun}$, hence have to be divided by N_{pix} in order to get the average intensity in the single pixel.

3. Results: signal associated with a SEP event

The typical distribution of spike noise due to cosmic rays (SEPs) hitting the COR1 detector for the selected event is shown in the right panel of *Figure 1* (running difference between the total brightness measured in 2 subsequent frames after the CME). This Figure shows that (as expected) spikes associated with SEPs are almost isotropically distributed on the detector, hence we may expect consequences over intensities summed over all the six considered angular sectors.

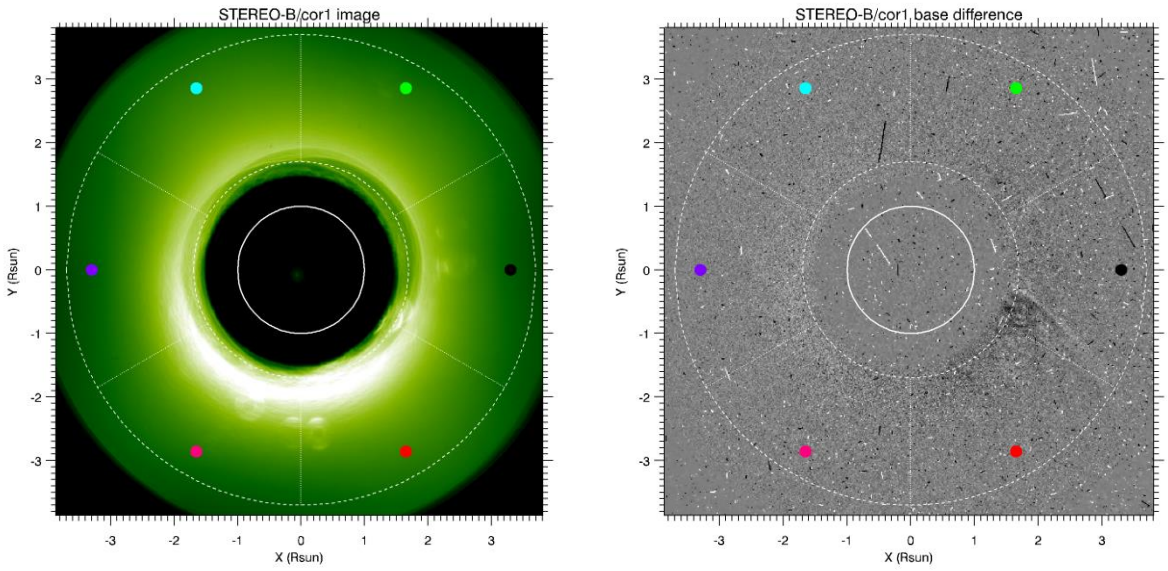

Figure 1: location of the 6 angular sectors selected to perform the test on the CME flag during the SEP bombardment of 21st March 2011. The level of noise associated with high energy particles impinging on the COR1 detector is shown in a standard (left) and a running difference (right) frame of total VL brightness. Filled circles show reference colors for the intensity curves measured in each angular sector and shown in the next plots.

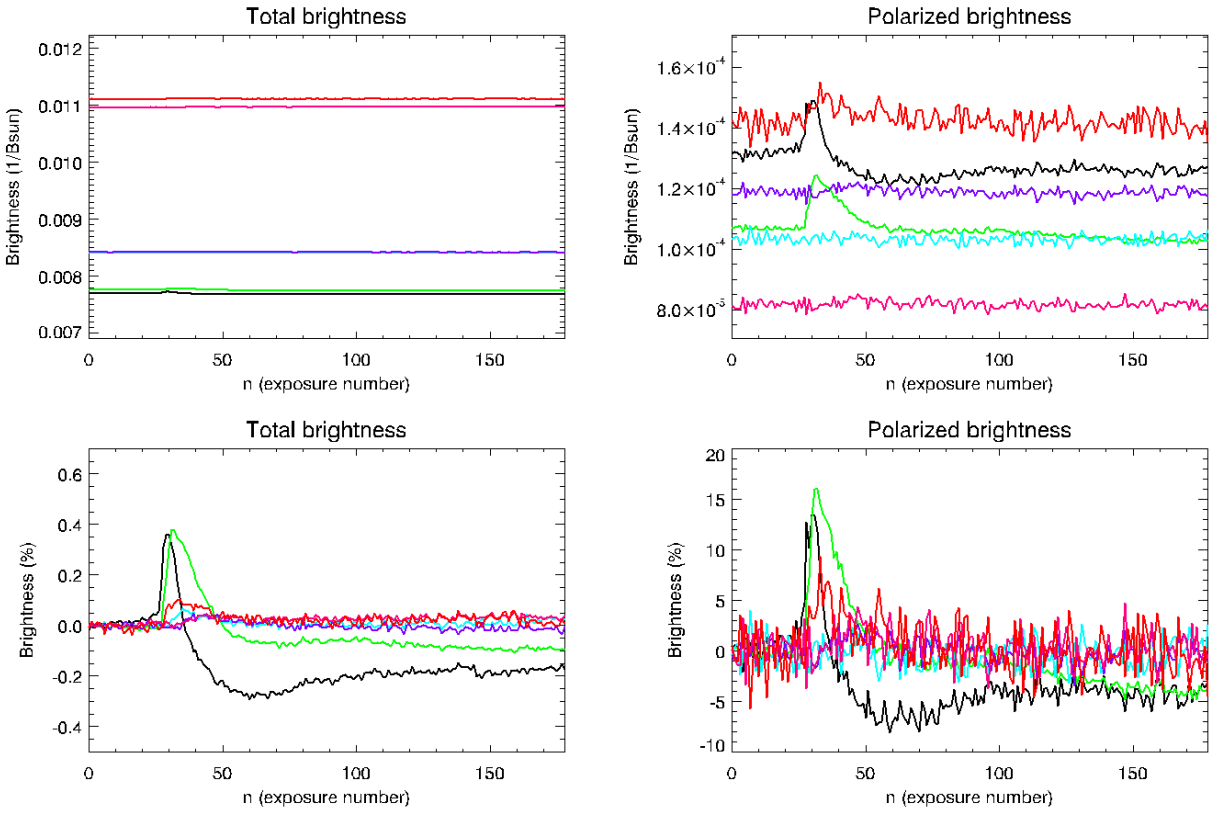

Figure 2, top: absolute ($1/B_{sun}$) intensity variations measured over the whole observation interval during the 21st March 2011 CME and the following SEP bombardment in the total (left) and polarized (right) brightness summed over different angular sectors (see Figure 1 for reference colors). Bottom: same as top for the relative (%) total (left) and polarized (right) intensity variations. Each exposure number corresponds to a 5 minutes time interval.

The evolution of total and polarized brightness measured over different angular sectors are shown in *Figure 2*, that shows a clear signature of the CME visible in the relative (%) brightness variations associated with

the West (black) and North-West (yellow) angular sectors. First of all, curves reported in *Figure 2* confirm results already obtained for the study of another "standard CME" (i.e. not an halo event): the total brightness variation is relatively small (not larger than 0.4%), while the polarization brightness variation is much larger (more than 15%). This is due to the geometry of Thomson scattering by coronal electrons, that gives a maximum degree of polarization for those electrons being closer to the plane of the sky: because the CME is a limb event, its degree of polarization is maximum.

Curves in *Figure 2* also show the after the occurrence of the CME and the associated flare there is no clear signature of increased noise associated with spikes. This is also confirmed by an estimate of signal variance before and after the CME in angular sectors affected by spikes and not affected by the eruption. The reason is that the intensity increase associated with these spikes is relatively very small.

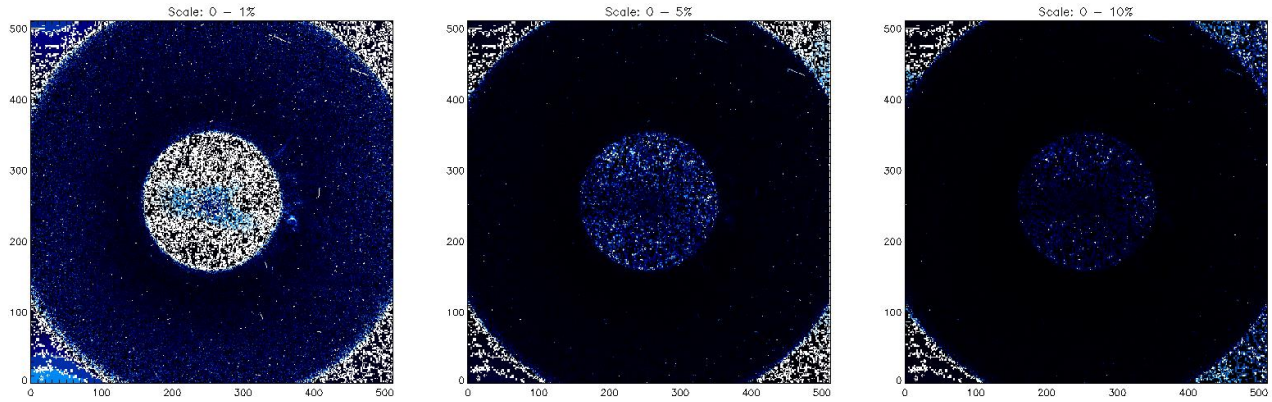

Figure 3: absolute value of relative difference $|I_2-I_1|/I_1$ between two subsequent exposures acquired on March 21st 2011 at 03:20:00 and 03:25:00 UT with the same orientation of linear polarizer (0°) showing the noise level associated with spikes for a color scale ranging between 0 and 1% (left), 5% (middle) and 10% right.

This point is better shown with panels given in *Figure 3*, that show the noise level associated with spikes in a couple of subsequent exposures acquired with the same orientation of the linear polarizer (in order to avoid coronal intensity variations related with the different polarization angles). These panels clearly show that all the spikes are basically below a peak intensity of about 10% relative to the surrounding coronal signal. Because the spikes have also a quite small area on the detector (a few pixels), it is not surprising that their contribution to the total emission is negligible once intensities are summed over different angular sectors. Notice that difference images in *Figure 3* were built with COR1 frames after radiometric calibration (COR1_CALIBRATE procedure), but this procedure is not taking care of cosmic rays.

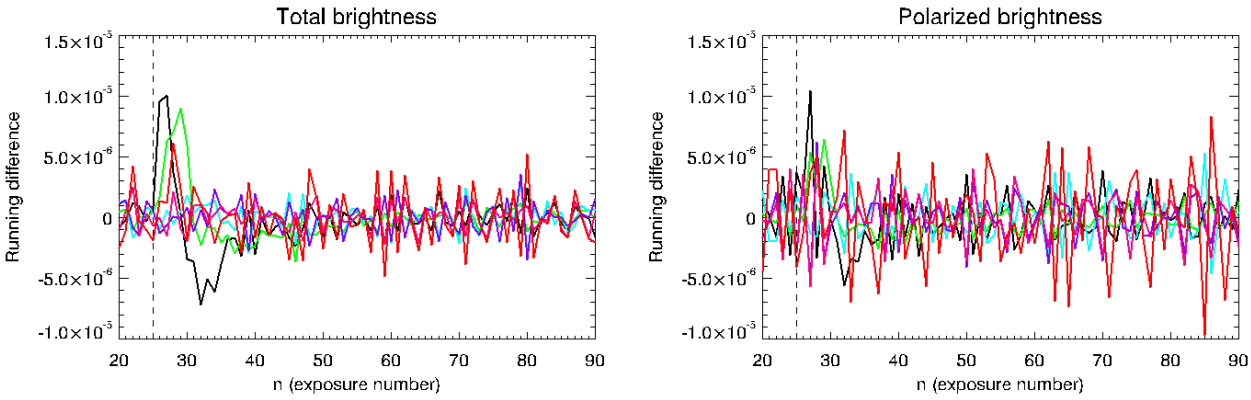

Figure 4: running differences measured over different angular sectors (see Figure 1 for reference colors) in the total (left) and polarized (right) brightness during the 21st March 2011 CME and the following SEP bombardment. CME start time is shown by the vertical dashed line. Each exposure number corresponds to a 5 minutes time interval.

The evolution of running differences in different angular sectors is shown in *Figure 4*, that basically confirms results already derived for the previous analysis of another "standard CME", i.e. that running differences are a fast and quick proxy for the determination of CME arrival time and that running difference peak values are comparable for total (*tB*) and polarized (*pB*) brightness.

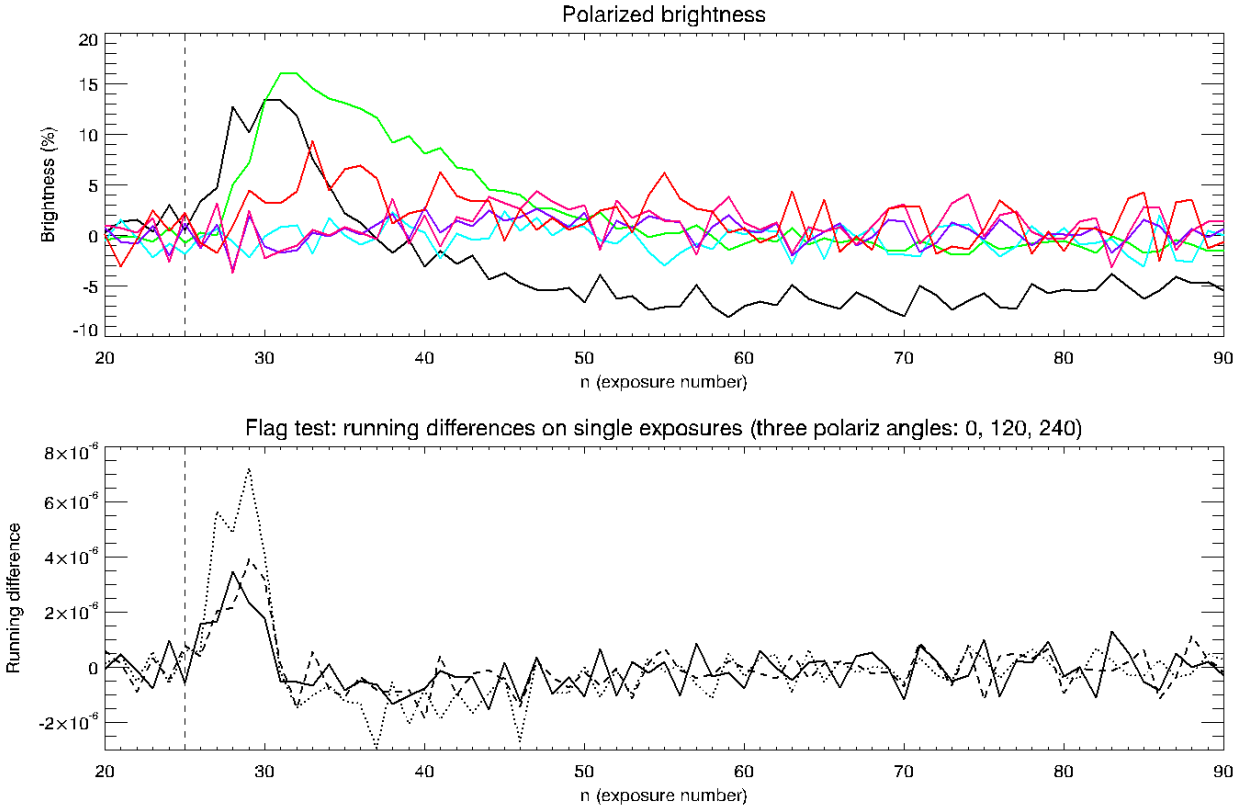

Figure 5, top: evolution of the relative (%) variations of polarized intensities measured over different angular sectors (see Figure 1 for reference colors) during the 21st March 2011 CME and the following SEP bombardment. Bottom: time evolution of running differences measured over the angular sector where the CME signal maximizes computed with images acquired with 3 different orientations of the linear polarizer. CME start time is shown by the vertical dashed line. Each exposure number corresponds to a 5 minutes time interval.

Nevertheless, due to computational limitations, the Metis Processing Unit will not be able to derive onboard images for the total and polarized brightness, hence the CME flag needs to deal with images

acquired with single orientation of the linear polarizer. Again, I confirm here for this second CME the result previously obtained for another event: as shown in *Figure 5* (bottom panel), looking at intensity evolution over the same angular sector crossed by the CME, the running difference peak value significantly depends on the considered orientation of the linear polarizer. Hence, images acquired with a single orientation of the linear polarizer cannot be directly employed to activate a CME flag.

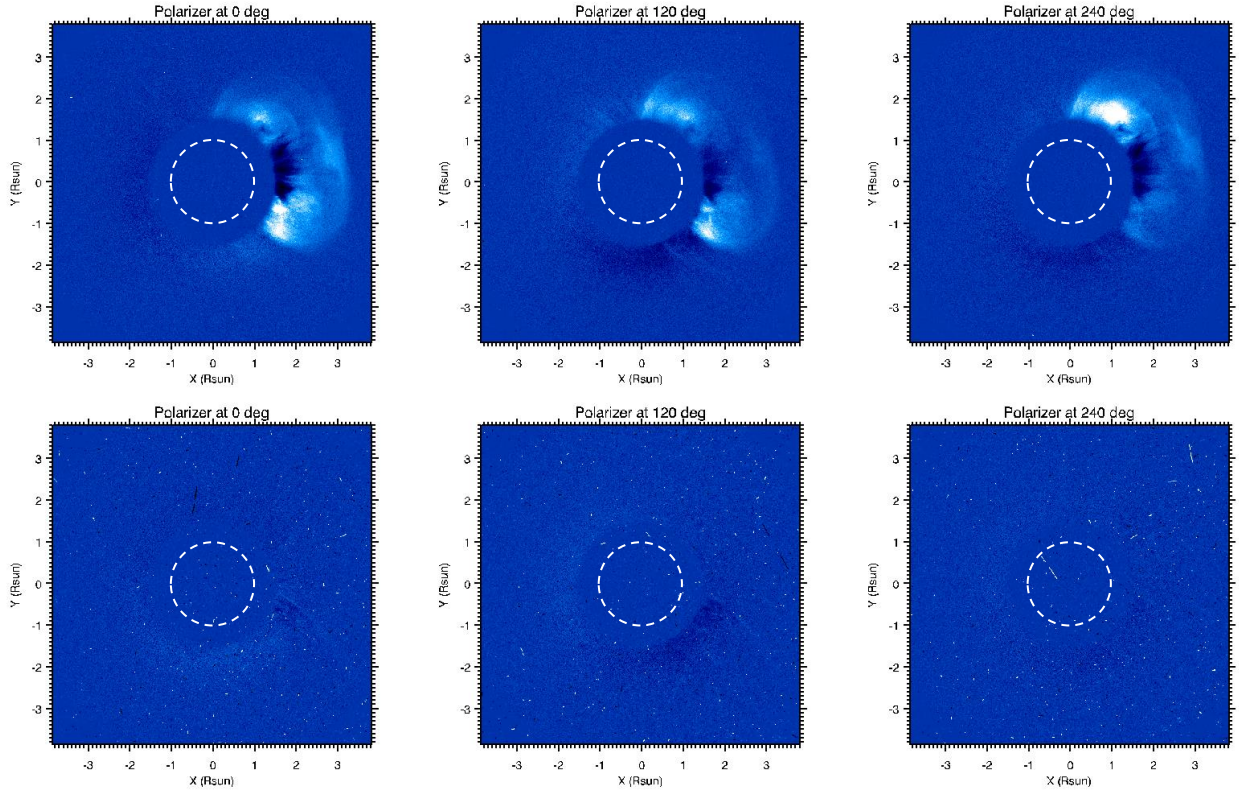

Figure 6, top: VL intensities observed during the CME by STEREO COR1 (pre-CME corona subtracted) with the linear polarizer oriented at 0° (left panel), 120° (middle panel) and 240° (right panel) with respect to the solar north observed on March 21st 2011, 02:40 UT. The range of color scale is the same for the three panels shown here (from -100 to +100). Bottom: same as top about one hour after the CME initiation.

This point is better explained again in *Figure 6* (top row), that shows with the same color scale the intensity of the CME (pre-CME corona subtracted) observed about at the same time (difference by 12 seconds between one exposure and the following one) with 3 different orientations (0°, 120° and 240°) of the linear polarizer. A comparison between the three panels shows the significant CME intensity variations simply associated with the orientation of the polarizer. For comparison, bottom panels in *Figure 6* show again the noise level associated with cosmic rays about one hour after the CME.

4. Results: signal associated with a planet transit

A typical COR1 frame during the transit of Jupiter across the instrument FOV is shown in *Figure 7* with an absolute (left) and base difference (right) image. The location of the planet is outlined by a yellow dashed circle in both images, while the planet path is shown by a solid white line. The planet appears in the 1024x1024 pixel frames as a circular spot with a diameter of about 6-7 pixels, hence covering an area of about 30-40 pixels (see also later on, *Figure 11*), and with a bi-Gaussian distribution of the intensity. Pixels at the location of the planet are not saturated in COR1 images. In any case, similarly to what previously described for the case of spikes, the relative intensity increase associated with the planet is significant, but

very limited in spatial extension. As a consequence the impact on the intensity averaged over different angular sectors is negligible.

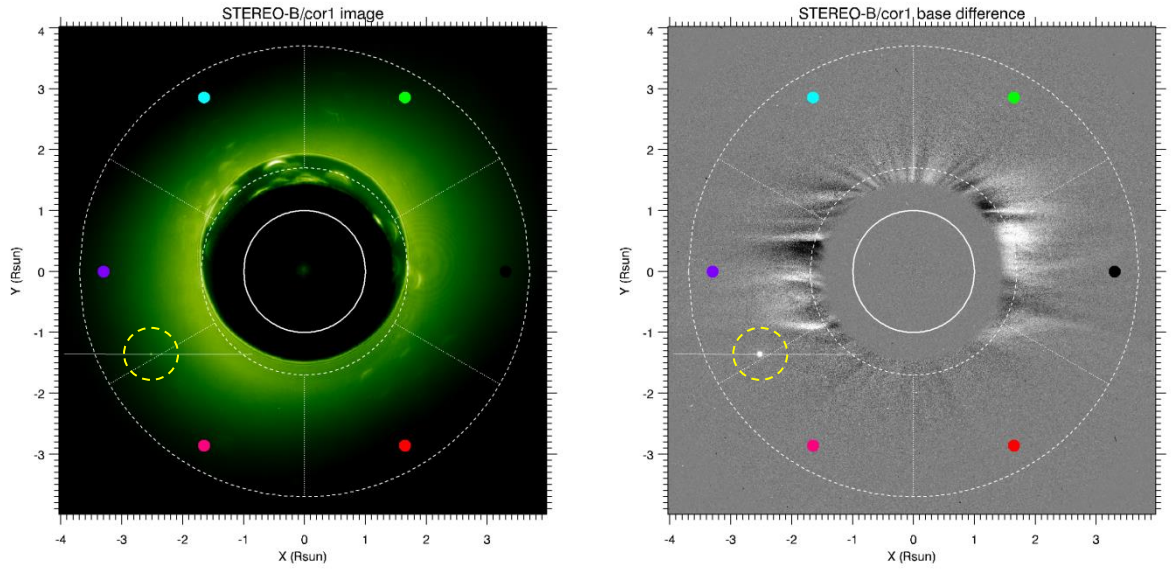

Figure 7: location of the 6 angular sectors selected to perform the test on the CME flag during the Jupiter's transit of March 15 – 16, 2009 (frame at 22:35 UT). The location of the planet in the COR1 detector (yellow dashed circle) and the path followed by the planed (solid white line) are shown in a standard (left) and a base difference (right) frame of total VL brightness (last frame before the planet arrival subtracted). Filled circles show reference colors for the intensity curves measured in each angular sector and shown in the next plots.

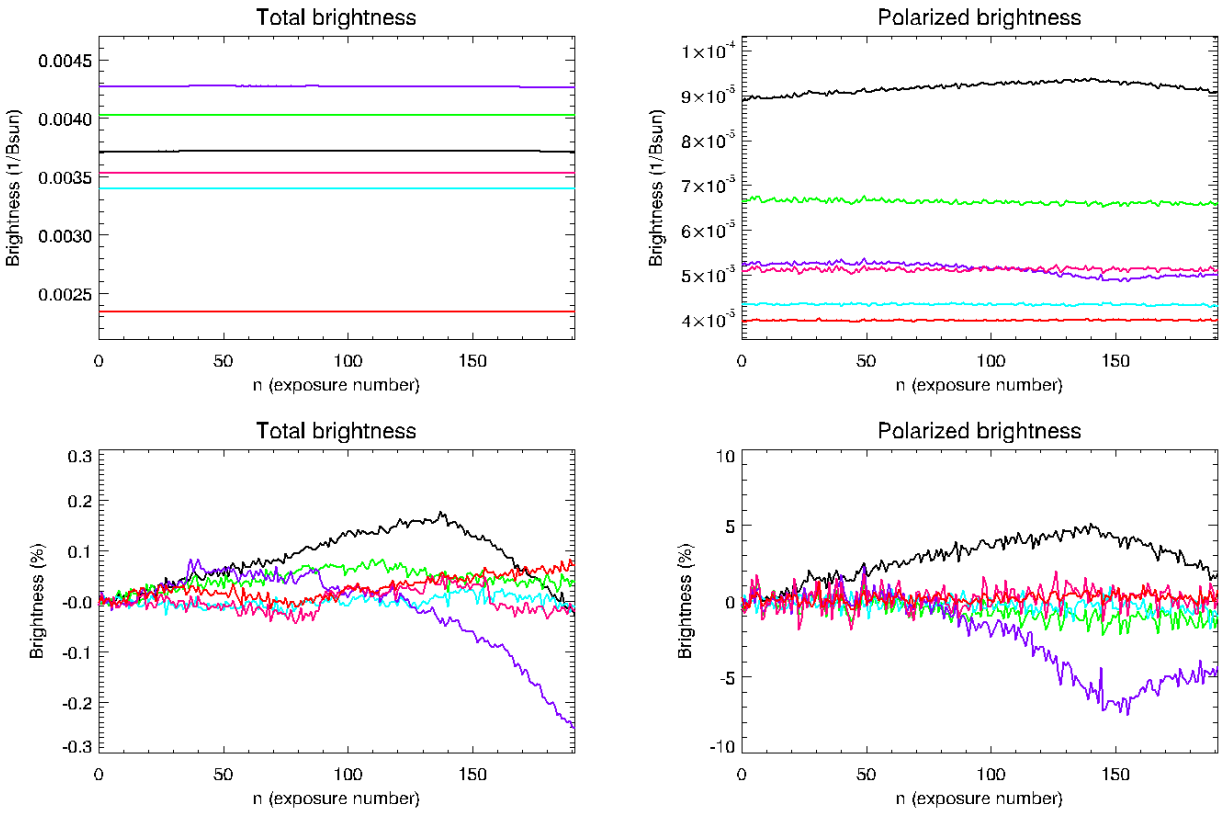

Figure 8, top: absolute (1/B_{sun}) intensity variations measured over the whole observation interval during the Jupiter's transit of March 15 – 16, 2009 in the total (left) and polarized (right) brightness summed over different angular sectors (see Figure 7 for reference colors). Bottom: same as top for the relative (%) total (left) and polarized (right) intensity variations. Each exposure number corresponds to a 5 minutes time interval.

This point is quantitatively shown in the top and bottom panels of *Figure 8*: the two angular sectors being crossed by the planet (East and South-East quadrants) in the time interval considered here (see *Table 1*) the average total brightness increase is barely visible and is on the order of about 0.05%. This is shown by the curves in the bottom left panel of *Figure 8*: as the planet enters in the East quadrant (exposure 35) the total brightness in this sector (blue curve) slightly increases by ~ 0.05%. Then, when the planet leaves the East quadrant and moves into the South-East quadrant (exposure 87) the same intensity increase is also observed (purple curve). These panels also show that no polarized emission is observed by the planet.

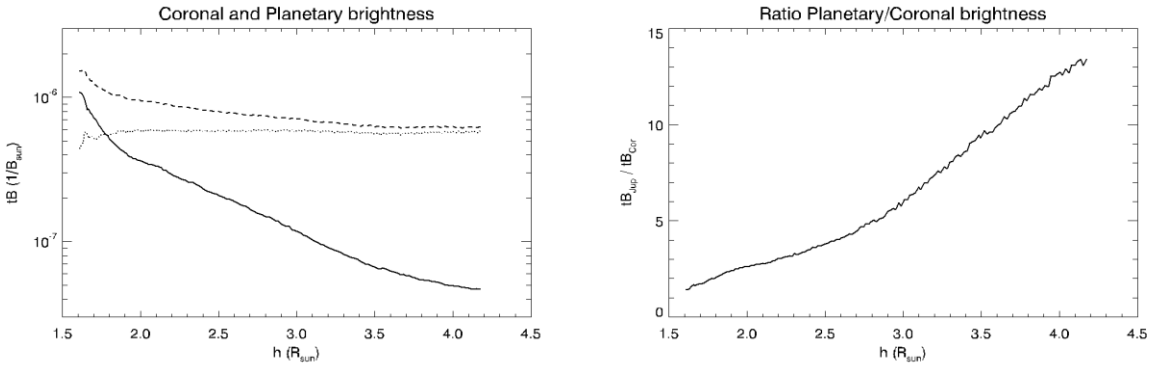

Figure 9, left: comparison between the total peak brightness (tB) measured by COR1 at the central location of Jupiter (dashed line) and in the surrounding corona (solid line) during the planetary transit at different projected altitudes, together with the difference between planetary and coronal brightness (dotted line). Right: ratio between the

Because the absolute planetary brightness could be useful as a future reference, in *Figure 9* (left panel) I show the evolution of the total peak brightness (units of $1/B_{sun}$) measured at the central location of the planet (dashed line) and in the corona a few pixels (4 pixels) away from the planet (solid line). A difference between these two curves shows (dotted line) that Jupiter had (for this specific observational case) a quite constant total peak brightness of about $tB_{Jup} = 5.7\times10^{-7}\ B^{-1}_{sun}$. A significant deviation from this constant value is observed only much closer to the inner occulter limit (below about 1.9 R_{sun}), suggesting the presence of vignetting contribution not properly corrected by the SECCHI calibration software. In *Figure 9* I also show that the ratio between the peak total brightness at the planet location and the brightness of the surrounding corona goes up with the projected altitude (because of the coronal intensity decrease), going from about $tB_{Jup} / tB_{Cor} \sim 2$ at 1.8 R_{sun} up to $tB_{Jup} / tB_{Cor} \sim 13$ at 4.0 R_{sun}, hence making the planet more than one order of magnitude brighter than the surrounding corona.

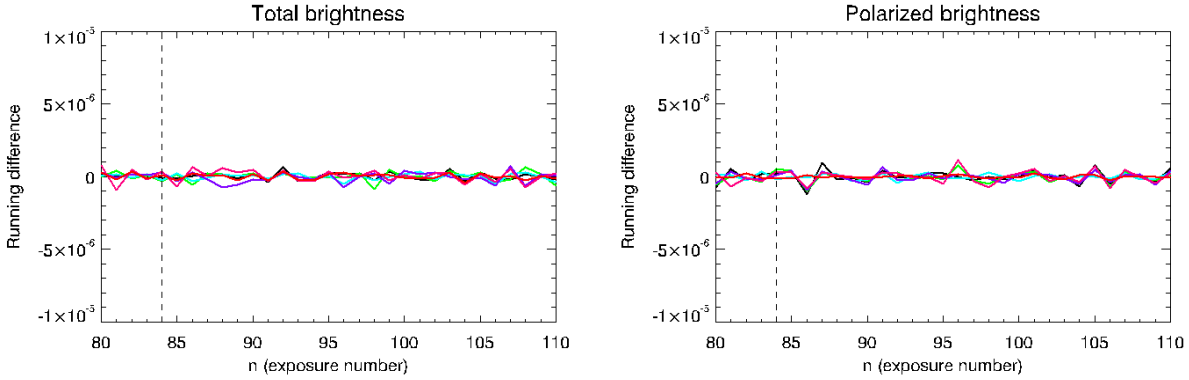

Figure 10: running differences measured over different angular sectors (see Figure 7 for reference colors) in the total (left) and polarized (right) brightness during the Jupiter's transit of March 15 – 16, 2009. Time when the planet enters in the COR1 FOV is shown by the vertical dashed line. Each exposure number corresponds to a 5 minutes time interval.

Because the Jupiter planet is very bright, but the images are not saturated, the measured Jupiter's intensity can be used to test the correctness of the COR1 coronagraph absolute calibration. At the time of the observations the Jupiter planet was at an heliocentric distance of about D_J = 5.0886 AU[1], while STEREO-B was at an heliocentric distance of D_{ST} = 0.9998 AU[2], hence (because Jupiter and STEREO-B were in opposition at that time) the total distance between Jupiter and the STEREO-B spacecraft was about D_{JST} = 6.0884 AU. The expected planetary intensity tB_J is then given by

$$tB_J = \pi A_J \left(\frac{R_{sun}}{D_J} \right)^2 \left(\frac{R_J}{s\, D_{JST}} \right)^2 B_{sun}$$

where R_{sun} = 6.965×10^5 km is the solar radius, R_J = 69911 km is the Jupiter radius and s is the size of a COR1 pixel in radians (s = 3.75 arcsec). Following the analysis performed by Dr. William Thompson for the COR1-A and –B intercalibration[3], the albedo was derived from the Jupiter Absolute Reflectivity Calibration Homepage[4]: it turns out that this is relatively flat over the COR1 bandpass, and has an average value of A_J = 0.505. With the above numbers I'd expect a planetary intensity of tB_{Jup} = 2.34×10^{-5} B^{-1}_{sun}. This number have to be compared with the total planetary brightness measured by integrating over all the pixels covered by the planet in the image. It turns out that tB_{Jup} = 6.3×10^{-6} B^{-1}_{sun}, hence about a factor 3.7 smaller than what expected: the reason for this discrepancy is unknown. The same technique could be easily applied to calibrate any coronagraphic image. Notice that the projected size of Jupiter is in agreement with all the above numbers: in fact, the expected projected diameter in pixels is given by d_J = atan(R_J/D_{JST}) / s ~ 4.21 pixels, as observed.

The absence of a significant emission once the intensity is averaged over different angular sectors implies also the absence of any feature in the running differences, as shown in *Figure 10*. This implies that the occurrence of planetary transits should not affects the CME detection algorithm. The planetary emission is almost totally unpolarized: this is shown in *Figure 11* where base difference images acquired with single orientation of the linear polarizer are shown for the whole field of view (top row) and for a zoom over the planet location (bottom row). Images acquired with different polarization states are almost identical. This is exactly opposite to what it was shown in the top panels of *Figure 6*, because (as mentioned) the CME emission is (on the contrary) highly polarized.

[1] As provided by http://www.imcce.fr/en/ephemerides/formulaire/form_ephepos.php for March 15, 2009, 22:35 UT.
[2] As provided by http://stereo-ssc.nascom.nasa.gov/where.shtml .
[3] http://secchi-ical.wikidot.com/cor1a-cor1b .
[4] http://charon.nmsu.edu/~nchanove/jupcal/jupitercal.html .

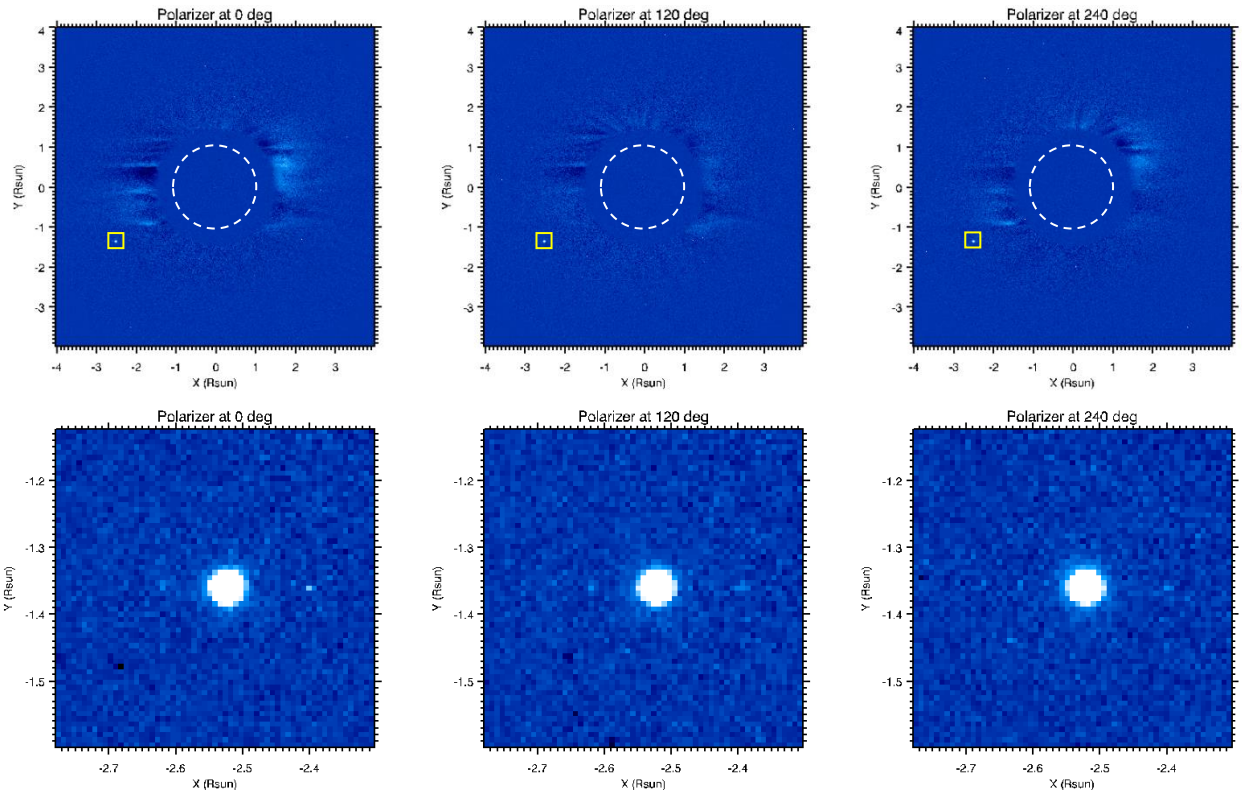

Figure 11, top: VL intensities observed during the Jupiter's transit by STEREO COR1 (pre-CME corona subtracted) with the linear polarizer oriented at 0° (left panel), 120° (middle panel) and 240° (right panel) with respect to the solar north. The range of color scale is the same for the three panels shown here (from -100 to +100). Bottom: same as top zoomed over the planet (yellow boxes in the top panels).

5. Results: signal associated with a comet transit

A typical COR1 frame during the transit of the Lovejoy comet is shown in *Figure 12* together with the location of the 6 angular sectors projected onto a total (left) and polarized (right) brightness images. From STEREO-B the comet orbital plane is seen almost edge-on: the comet enters the FOV from the bottom-right corner (thus crossing the South-West angular sector) on December 15th 2011 around 21:05 UT, starts to enter in the South-West sector at 21:50 UT (exposure 70), and then moves sunward almost radially starting to leave the angular sector on December 16th at 23:05 UT (exposure 84) and eventually disappearing behind the COR1 occulter. The comet then reappears back on December 16th 2011 around 05:25 UT after crossing its perihelion and then moves anti-sunward in the South-West direction expanding at slightly smaller latitude, thus entering in the West angular sector.

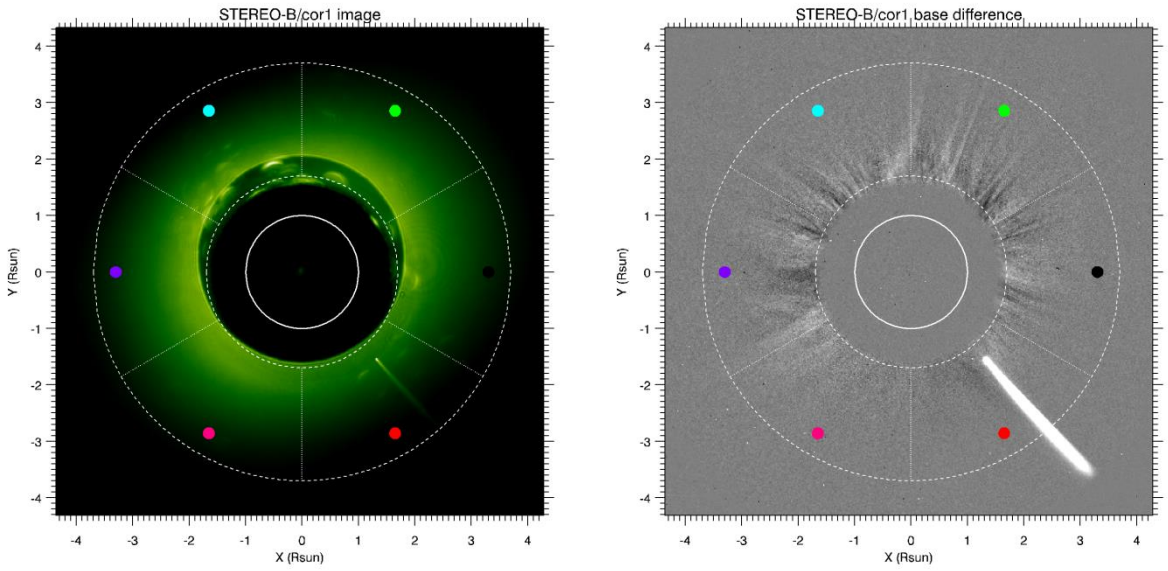

Figure 12: location of the 6 angular sectors selected to perform the test on the CME flag during the Lovejoy comet transit of December 15 – 16, 2011 (frame at 22:50 UT). The location of the comet in the COR1 detector is shown in a standard (left) and a base difference (right) frame of total VL brightness (last frame before the comet arrival subtracted). Filled circles show reference colors for the intensity curves measured in each angular sector and shown in the next plots.

The evolution of total (*tB*) and polarized (*pB*) brightness averaged over different angular sectors is shown in *Figure 13*: the arrival of the comet corresponds to a significant increase in the total brightness, with a maximum relative increase of about 1.3%, hence much larger than what typically observed during CMEs (0.4% - 0.5%). This emission is (similarly to what described for the transit of Jupiter) almost unpolarized, hence no significant pB intensity variation is observed during the comet transit (*Figure 13*, bottom right panel). As for the case of the planet transit described above, even the signal associated with this comet is not saturated. In fact the absolute intensity increase is not significantly larger than what observed for the case of planetary transit: for example the maximum value of the ratio between cometary and coronal emissions observed in the frame shown in *Figure 12* is tB_{Com} / tB_{Cor} ~ 3.7. Nevertheless cometary emission occupies a significant fraction of the detector (about 2030 pixels in the frame shown in *Figure 12*), making the brightness variation averaged over the angular sector significant.

This is also shown by sequences of running differences (*Figure 14*) as derived for the total (left) and polarized (right) brightness in each angular sector. The observed peak value of running difference for total brightness is on the same order than what observed during standard CMEs, while no signal is detected in polarized brightness.

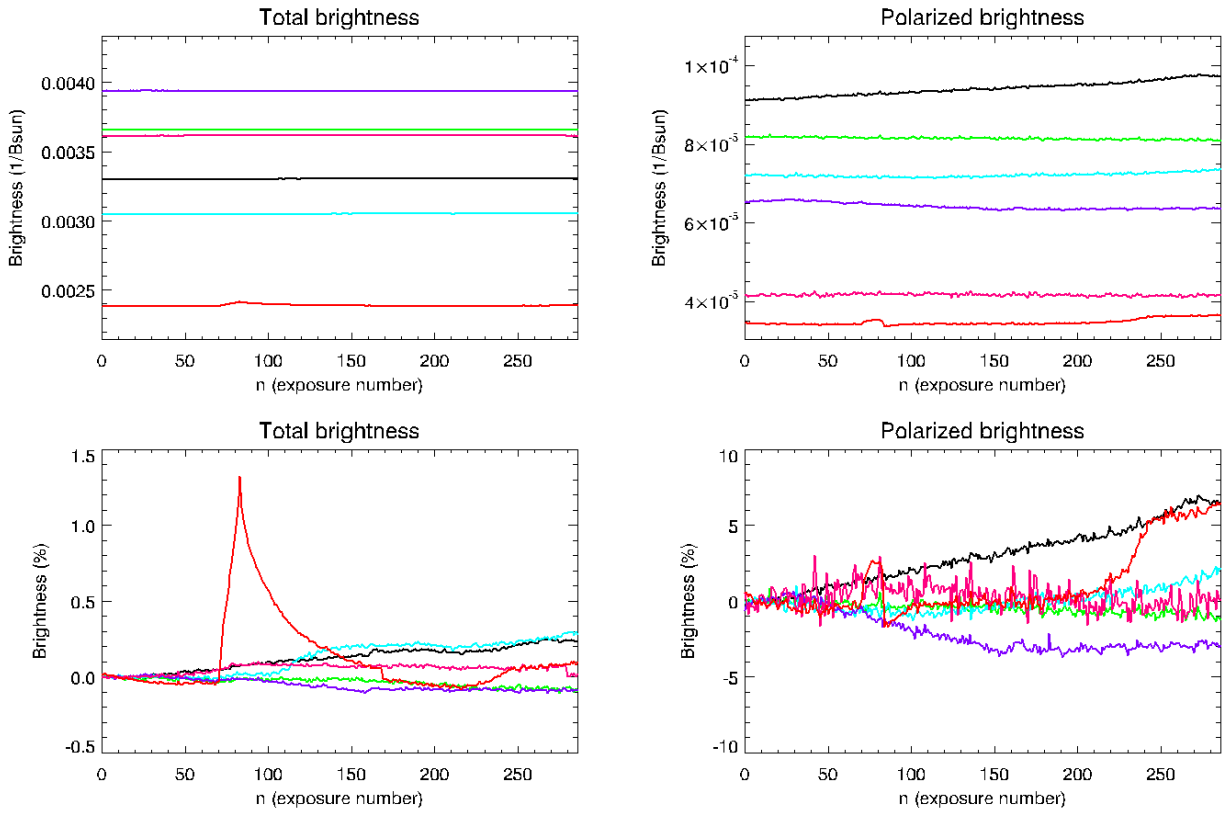

Figure 13, top: absolute ($1/B_{sun}$) intensity variations measured over the whole observation interval during the Lovejoy comet transit of December 15 – 16, 2011 in the total (left) and polarized (right) brightness summed over different angular sectors (see Figure 12 for reference colors). Bottom: same as top for the relative (%) total (left) and polarized (right) intensity variations. Each exposure number corresponds to a 5 minutes time interval.

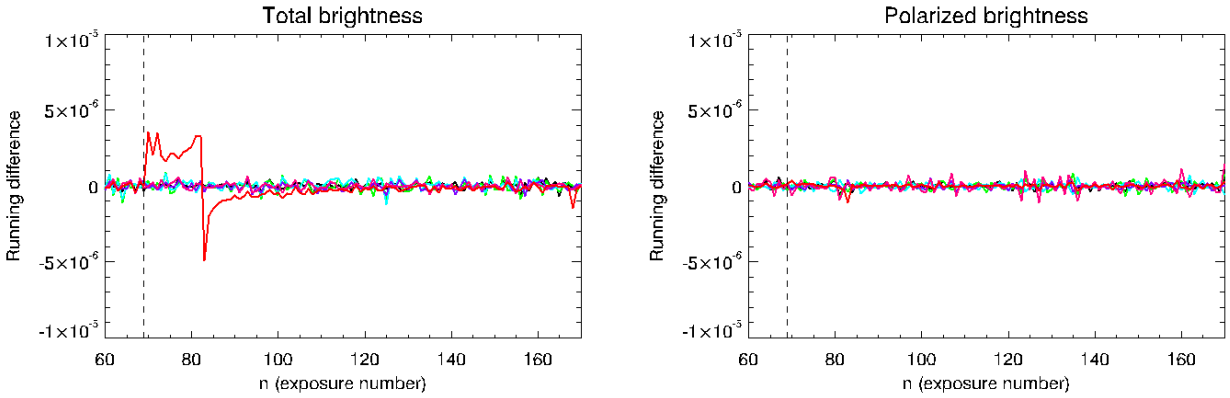

Figure 14: running differences measured over different angular sectors (see Figure 12 for reference colors) in the total (left) and polarized (right) brightness during the Lovejoy comet transit of December 15 – 16, 2011. Time when the comet enters the COR1 FOV is shown by the vertical dashed line. Each exposure number corresponds to a 5 minutes time interval.

The absence of polarized emission from the comet is also shown in top and bottom panels of *Figure 15*, to be also compared with similar panels in *Figure 6* and *Figure 11*: different from the case of CME observations, and similarly to the case of planet observations, cometary images acquired with different orientations of the linear polarizer are almost identical.

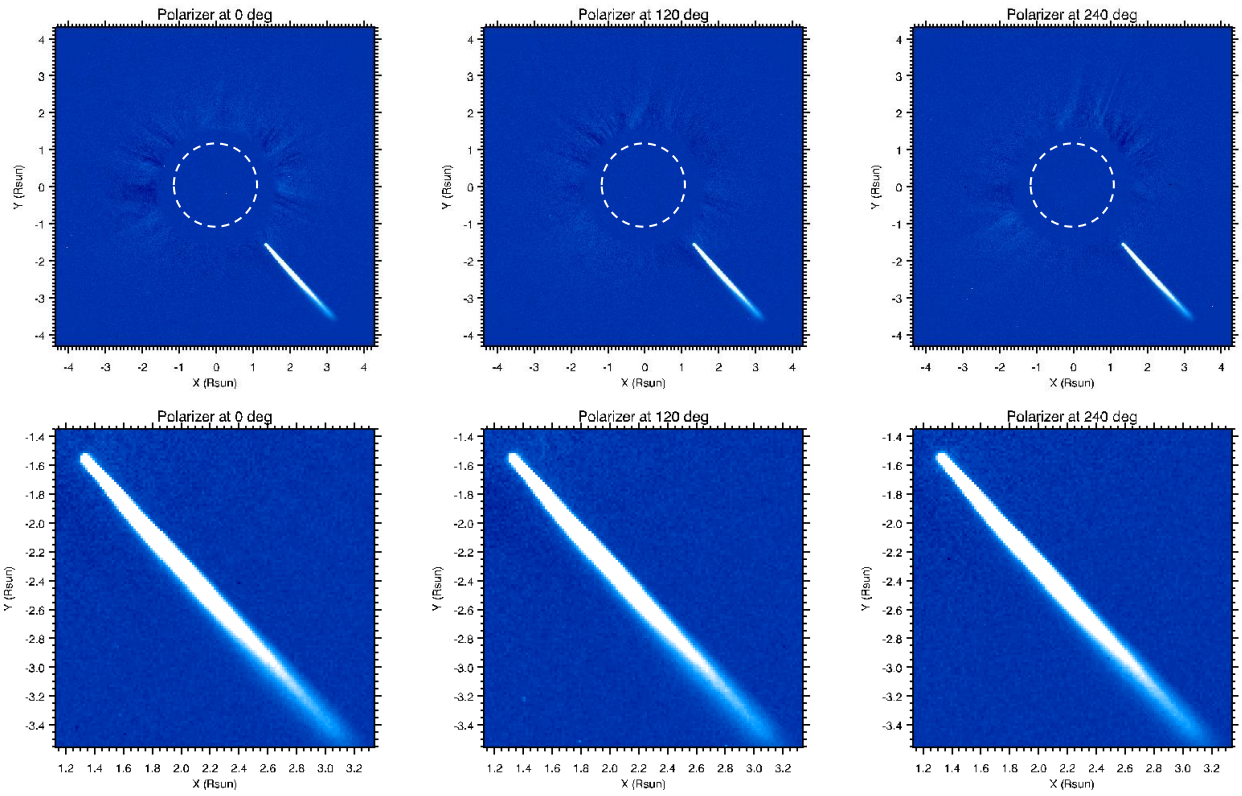

Figure 15, top: VL intensities observed during the Lovejoy comet transit by STEREO COR1 (pre-CME corona subtracted) with the linear polarizer oriented at 0° (left panel), 120° (middle panel) and 240° (right panel) with respect to the solar north. The range of color scale is the same for the three panels shown here (from -100 to +100). Bottom: same as top zoomed over the comet.

6. Comparison between STEREO/COR1 and SOHO/LASCO intensities

It is very important to point out that all the above results were obtained with data acquired by the COR1 coronagraphs onboard STEREO, which are very different from LASCO coronagraphs onboard SOHO. First of all, the instruments have very different bandpasses: COR1 has a quite narrow bandpass 10 nm wide, centered on the Hα line at 656 nm, while LASCO has (with the "orange" filter) a much broader bandpass between 520-640 nm (hence 120 nm wide). Hence, there is also no overlap between the two bandpasses. Second: the instruments have very different signal-to-noise ratio (SNR) and sensitivities. The COR1 telescope is occulted at 1.5 solar radii, while C2 is occulted at 2.2 solar radii, thus COR1 has much larger background corona and stray light to deal with. In particular, the large COR1 stray light contribution is basically due to 1) smaller occulter dimensions, and 2) larger scattering from the exposed lenses[5]. Moreover COR1 has an exposure time of 1.7 seconds, to be compared with the C2 exposure time of about 19 seconds. Once this factor ~ 11.2 between the C2 and COR1 exposure times is combined with the factor ~ 12 between the C2 and COR1 bandpass extensions, this results in a much weaker noise in C2 images with respect to COR1 (for a significant part of the above conclusions I acknowledge comments received by Dr. A. Vourlidas).

Because the COR1 images have a much lower SNR with respect to C2 images, also the relative variation of visible light intensity detected during CMEs with COR1 or C2 are very different. In order to better demonstrate this point, I analyzed the data relative to a significant CME that occurred on December 31, 2007 (starting around 01:00 UT). The event (shown in *Figure 16*) was observed by COR1 and C2 telescopes on the South-East quadrant and occurred when the separation angle between STEREO-B and SOHO was

[5] A. Vourlidas, private communication.

22.80°, while the separation angle between STEREO-A and SOHO was 21.17°, hence in first approximation the C2 and COR1 coronagraphs are looking at the CME from the same point of view.

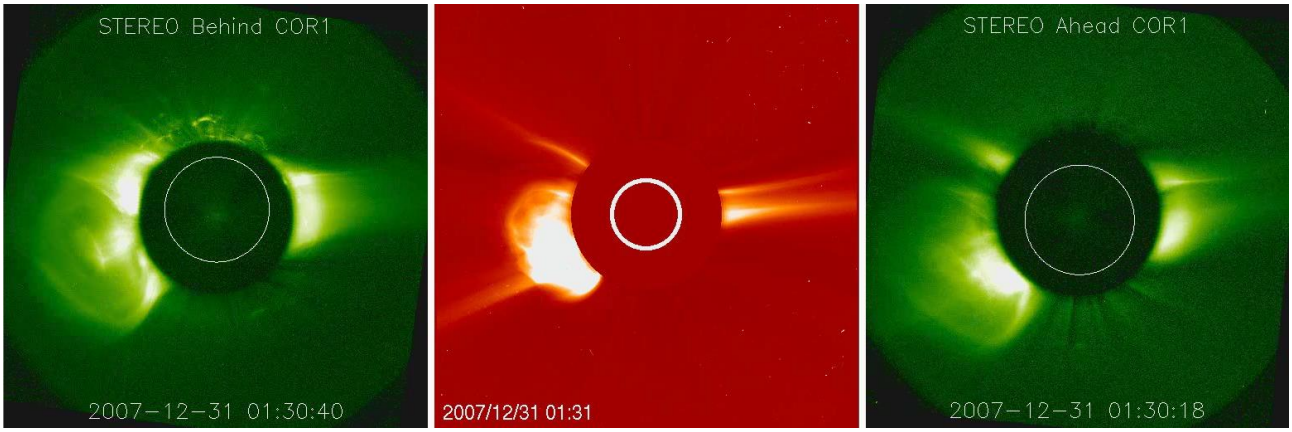

Figure 16: the December 31, 2007 CME as seen by COR1 onboard STEREO-B (left) and –A (right) and by LASCO-C2 onboard SOHO (middle).

In order to compare the evolution of visible light brightness detected by different instruments, I modified the range of heliocentric distances of the angular sectors in order to cover the same interval with different instruments. Basically, the lower edge (dictated by the location of the LASCO-C2 inner occulter edge) was placed at 2.2 solar radii, while the higher edge (dictated by the outer occulter edge of the COR1 telescope onboard STEREO-A, i.e. the spacecraft closer to the Sun) was placed at 3.7 solar radii (see *Figure 17*).

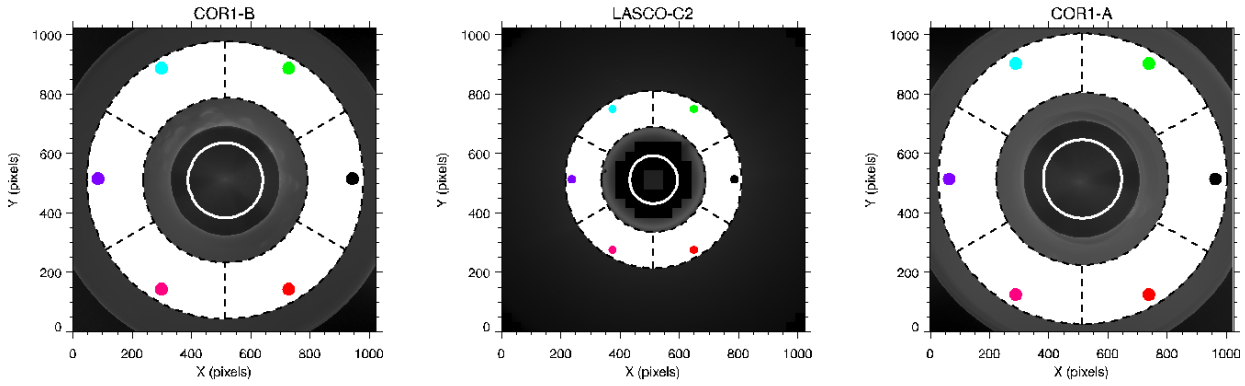

Figure 17: the location of angular sectors used for the comparison between C2 and COR1 intensity variations; filled circles show reference colors for the intensity curves measured in each angular sector and shown in the next plot.

In the time interval between 00:00 and 04:06 UT the LASCO-C2 instrument acquired 10 unpolarized exposures with the standard “orange” filter (540-640 nm), while the twin COR1 instruments acquired 48 triplets of linearly polarized images. A polarized sequence was also acquired by LASCO-C2 between 02:54-03:04 UT, but the CME was already out of the COR1 field of view at that time. As done for the analysis described before, for each COR1 triplet the total brightness was derived with standard routine provided by the SECCHI package and its relative variations averaged over different angular sectors are compared with relative variations of LASCO-C2 intensities.

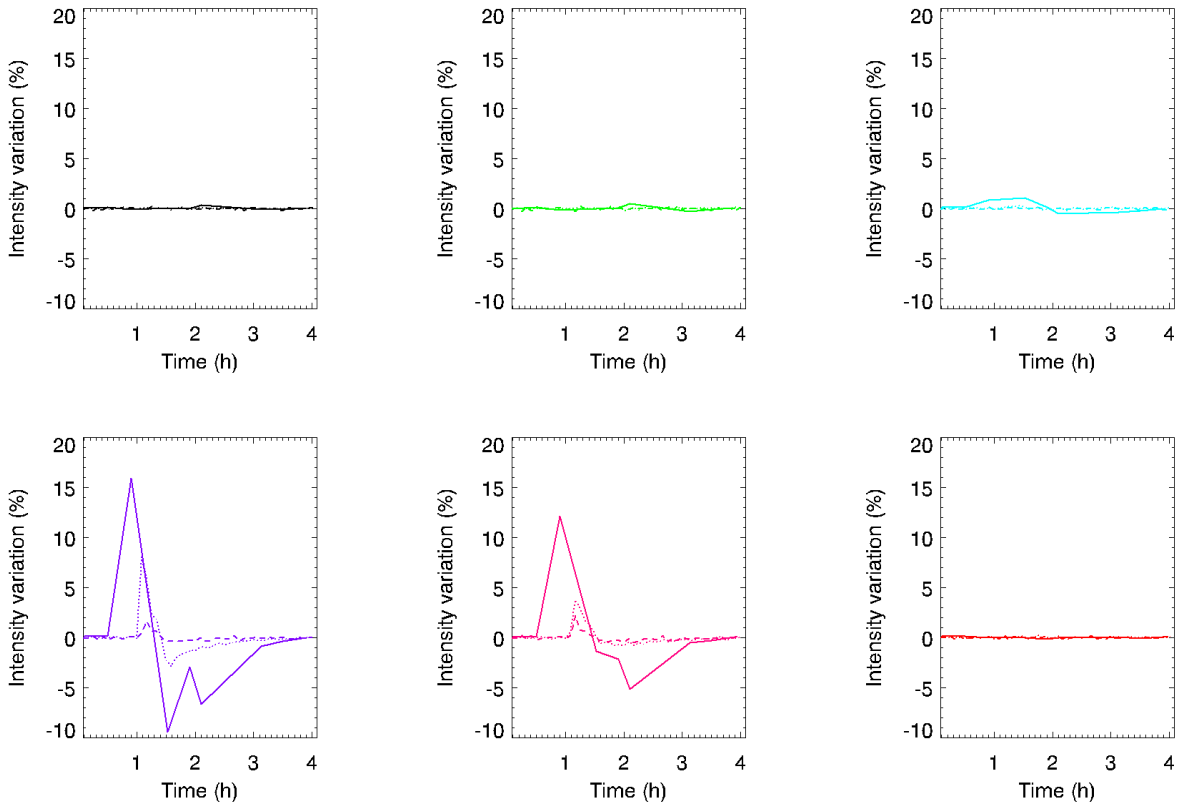

Figure 18: evolution of relative running differences $(I_{i+1} - I_i)/I_i$ *as observed over different angular sectors (see Figure 17 for reference colors) by using data acquired by LASCO-C2 (solid) and STEREO-COR1 (dotted and dashed). The COR1 intensity variations have been multiplied by a factor 10 in order to be visible in the same plot with C2 intensity variations.*

Resulting evolution of relative running differences $(I_{i+1} - I_i)/I_i$ are shown in *Figure 18* for different instruments; these plot show that the same CME corresponds to a relative intensity variation by more than 15% in C2 data (solid lines), and by less than 1% in COR1 data (dotted and dashed lines, multiplied by a factor 10). Hence, there is more than a factor ~ 15 between relative intensity variations observed by C2 and COR1 for the same event.

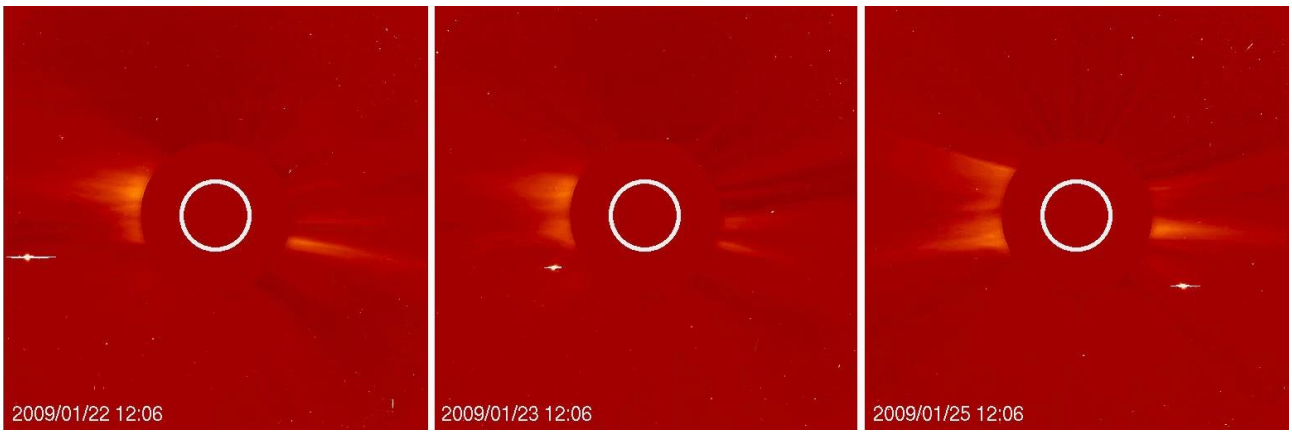

Figure 19: sequence of LASCO-C2 images during the Jupiter's transit on January 2009.

Notice that the same difference is also present for the case of planetary transits: for instance, about two months before the transit in COR1-B field of view described above, the Jupiter planet also crossed the

LASCO-C2 field of view (approximately between January 22, 06:30 and January 26, 14:06 UT). During this time interval Jupiter was at an heliocentric distance of about D_J = 5.105 AU[6], hence the distance from SOHO was about was D_{JSO} = 0.974 + 5.105 = 6.079 AU very close to the distance from STEREO-B two months later (D_{JST} = 6.0884 AU): hence, the intrinsic planetary intensity tB_J was approximately the same. Nevertheless, while (as mentioned) COR1 frames are not saturated at the pixel location of Jupiter, C2 frames are significantly saturated, as also shown by the presence of a bright nearly horizontal saturation spike (see *Figure 19*). This clearly demonstrates how big is the difference between the responses and sensitivities of COR1 and C2 telescopes to the same visible light source (Jupiter in this case).

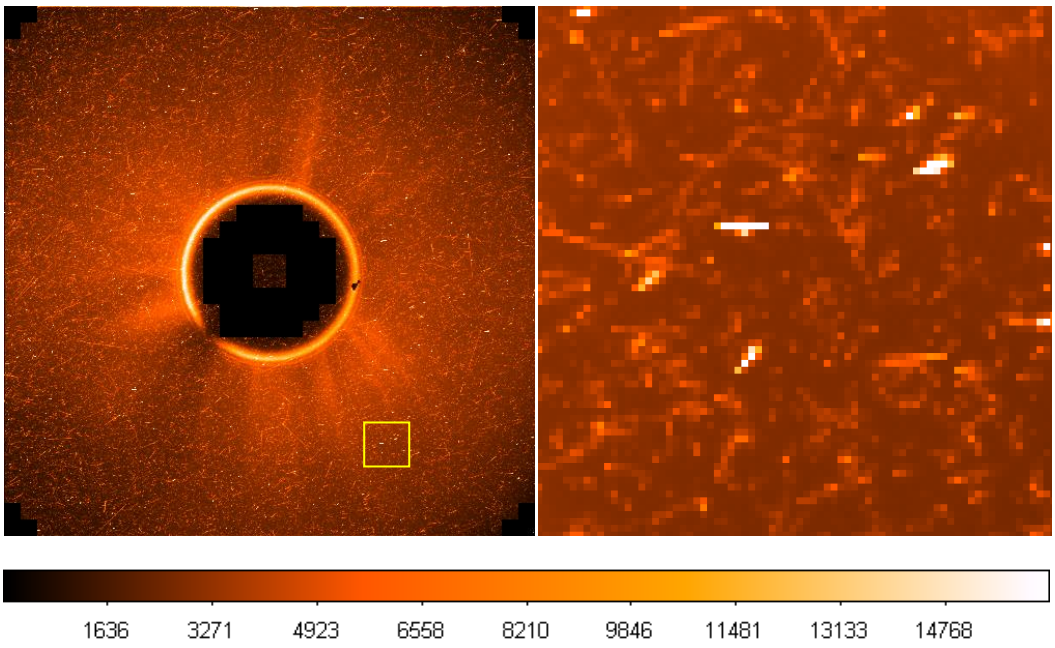

Figure 20: example of a LASCO-C2 image acquired after a solar flare (09/11/2000, 00:26 UT; color scale in DN, linear from 0 to 16383 = 2^{14} – 1); the noise level due to spikes has to be compared with what shown in Figure 3 for COR1 data relative to another event.

The big difference in the C2 and COR1 exposure times is probably also the explanation for the big difference in the level of spike noise observed during SEP bombardment events. In fact, spikes due to cosmic rays or SEPs are accumulated on the C2 detector over an integration time which is ~ 11.2 times larger than the COR1 integration time, thus producing a much stronger effect (see *Figure 20*, left panel). Notice that even in C2 images only a very small fraction of cosmic rays corresponds to a real saturation of the detector (see *Figure 20*, right panel).

7. Summary and conclusions

In this work I analyzed the consequences on VL coronagraphic images of the occurrence of spikes due to a SEP event, of a planet (Jupiter) transit and of a comet (Lovejoy) transit. Results based on sequences acquired by STEREO/COR1 telescope show that:

- Signal associated with spikes due to cosmic rays and to the planetary transit is significant, but occupies a very small fraction of the angular sector area, thus leading to a negligible contribution of the running differences.

[6] As provided by http://www.imcce.fr/en/ephemerides/formulaire/form_ephepos.php for March 15, 2009, 22:35 UT.

- Signal associated with the comet transit is not larger than what observed during the planet transit, but occupies a much larger area on the detector, thus becoming significant once averages over angular sectors are computed.

In conclusion, as far as images that will be provided by Metis on Solar Orbiter will be similar to those actually provided by COR1 on STEREO, an algorithm designed to automatically detect CMEs will be not affected by spikes and planet transits, while bright comets (like the Lovejoy) will be identified as a CME. It is likely that this will not happen for sungrazing comets, whose extension on the detector is much smaller.

There are at least two possible simple ways to automatically distinguish between a comet and a CME:

1) To compute the average intensity over 16 and not 8 angular sectors, by placing 8 inner sectors at lower altitudes (closer to the inner occulter edge) and 8 outer sectors higher up (closer to the outer occulter edge). A CME will rise the flag first in the inner and then in the outer sectors, while the opposite will occur for a comet.
2) To take into account that, opposite to what happens for CMEs, the cometary emission is not significantly polarized, thus a CME corresponds to different intensity increases in the same angular sector depending on the orientation of the linear polarizer (*Figure 6*), while this is not the case for a comet (*Figure 15*).

The second point suggest a simple strategy to distinguish between a comet and a CME: once the CME flag is raised, the algorithm should compute (only in the angular sector where the flag was activated) the difference between emissions measured in the same sectors with different orientations of the linear polarizer. If this difference is significant (i.e. larger than a threshold to be defined) the event is a CME, otherwise the event is a comet. Nevertheless, this strategy could work only for “standard CMEs”, but not for “halo CMEs” which are very weakly polarized.

Nevertheless all the above conclusions are based on the analysis of data acquired by the COR1 telescopes onboard STEREO. A comparative analysis conducted on STEREO/COR1 and SOHO/LASCO-C2 images relative to observation of the same astronomical objects (a CME and a planet) shows significant differences in the relative variations of the visible light intensities. In particular, relative running differences computed with LASCO-C2 are about a factor ~ 15 (or event more) than those computed with COR1 data. These differences suggest that a reliable value of the threshold value for the activation of the Metis “CME flag” likely will be possible only after launch of Solar Orbiter, when the first real data will be available. Moreover, likely due to the much longer integration time, C2 images are more heavily affected by spikes due to cosmic rays.